

# Systematic investigation of synthetic polyelectrolyte bottlebrush solutions by neutron and dynamic light scattering, osmometry, and molecular dynamics simulation

Cite as: J. Chem. Phys. **152**, 194904 (2020); <https://doi.org/10.1063/5.0007271>

Submitted: 10 March 2020 . Accepted: 03 May 2020 . Published Online: 21 May 2020

Ferenc Horkay , Alexandros Chremos , Jack F. Douglas , Ronald L. Jones, Junzhe Lou, and Yan Xia



View Online



Export Citation



CrossMark

## ARTICLES YOU MAY BE INTERESTED IN

[Dynamic heterogeneity and collective motion in star polymer melts](#)

The Journal of Chemical Physics **152**, 054904 (2020); <https://doi.org/10.1063/1.5135731>

[Effect of dissolved salt on the anomalies of water at negative pressure](#)

The Journal of Chemical Physics **152**, 194501 (2020); <https://doi.org/10.1063/5.0002745>

[Pair-distribution function of active Brownian spheres in two spatial dimensions: Simulation results and analytic representation](#)

The Journal of Chemical Physics **152**, 194903 (2020); <https://doi.org/10.1063/1.5140725>

Lock-in Amplifiers  
up to 600 MHz



# Systematic investigation of synthetic polyelectrolyte bottlebrush solutions by neutron and dynamic light scattering, osmometry, and molecular dynamics simulation

Cite as: *J. Chem. Phys.* **152**, 194904 (2020); doi: [10.1063/5.0007271](https://doi.org/10.1063/5.0007271)

Submitted: 10 March 2020 • Accepted: 3 May 2020 •

Published Online: 21 May 2020



View Online



Export Citation



CrossMark

Ferenc Horkay,<sup>1,a)</sup>  Alexandros Chremos,<sup>1,a)</sup>  Jack F. Douglas,<sup>2,a)</sup>  Ronald L. Jones,<sup>2</sup> Junzhe Lou,<sup>3</sup> and Yan Xia<sup>3</sup>

## AFFILIATIONS

<sup>1</sup>Section on Quantitative Imaging and Tissue Sciences, Eunice Kennedy Shriver National Institute of Child Health and Human Development, National Institutes of Health, Bethesda, Maryland 20892, USA

<sup>2</sup>Materials Science and Engineering Division, National Institute of Standards and Technology, Gaithersburg, Maryland 20899, USA

<sup>3</sup>Department of Chemistry, Stanford University, Stanford, California 94305, USA

<sup>a)</sup>Authors to whom correspondence should be addressed: [horkayf@mail.nih.gov](mailto:horkayf@mail.nih.gov); [chremos@mail.nih.gov](mailto:chremos@mail.nih.gov); and [jack.douglas@nist.gov](mailto:jack.douglas@nist.gov)

## ABSTRACT

There is a great interest in the synthesis and characterization of polyelectrolytes that mimic naturally occurring bottlebrush polyelectrolytes to capitalize on the unique properties of this class of macromolecules. Charged bottlebrush polymers form the protective mucus layer in the lungs, stomach, and orifices of animals and provide osmotic stabilization and lubrication to joints. In the present work, we systematically investigate bottlebrush poly(sodium acrylates) through a combination of measurements of solution properties (osmometry, small-angle neutron scattering, and dynamic light scattering) and molecular dynamics simulations, where the bottlebrush properties are compared in each case to their linear polymer counterparts. These complementary experimental and computational methods probe vastly different length- and timescales, allowing for a comprehensive characterization of the supermolecular structure and dynamics of synthetic polyelectrolyte bottlebrush molecules in solution.

<https://doi.org/10.1063/5.0007271>

## INTRODUCTION

Bottlebrush polymers are comprised of densely grafted chains tethered to a polymer backbone. These polymers differ strongly from their linear polymer counterparts not only in their architecture but also in their physical properties that are primarily controlled by the length of the main and side chains, the grafting density, and the steric repulsion of the side chains. For example, entanglement interactions have been found to be greatly diminished in neutral bottlebrush polymers,<sup>1</sup> enabling the fabrication of materials for many applications, where soft materials of high mechanical stability are required, e.g., soft contact lenses.

Recently, this class of materials has attracted a great deal of attention for both fundamental studies and applications. Bottlebrush polymers are used as drug delivery agents, surface coatings, modifiers of rheological properties, etc.<sup>2–6</sup> In addition to applications, bottlebrush architectures are essential components of living systems. Typical examples are cartilage and viscoelastic mucin layers forming protective coatings in the lungs, orifices, and digestive tracts of animals. In the cartilage extracellular matrix (ECM), the major proteoglycan component is the bottlebrush-shaped aggrecan molecule.<sup>7,8</sup> In the presence of hyaluronic acid and link protein, a secondary bottlebrush architecture is formed in which aggrecan molecules are condensed on a hyaluronic acid chain. The aggrecan/hyaluronic acid complexes are enmeshed in

an interpenetrating collagen matrix, and these molecules govern the load bearing properties of the cartilage. Furthermore, the bottlebrush architecture has excellent lubrication properties, protecting the articulating bone surfaces against frictional damage.<sup>9,10</sup>

Despite the tremendous potential of bottlebrush polymers in both materials science and biology, the effects of the charged bottlebrush topology on the physicochemical behavior of their solutions have not yet been fully elucidated.<sup>11</sup> For example, the effect of charges on the conformation of bottlebrush molecules is poorly understood. The effect of ions is particularly important in the biological milieu where both mono- and divalent counterions are present. Elucidating these basic physical properties is of fundamental importance to fully understand the importance of the bottlebrush architecture for designing advanced materials and understanding basic molecular physics underlying certain biological functions.

We aim to determine the effects of the ionic environment on the solution structure of bottlebrush sodium polyacrylates in which the length of both the main chain (polymer backbone) and the side chain was varied. We report systematic measurements using complementary experimental techniques, small angle neutron scattering (SANS), dynamic light scattering (DLS), and osmotic pressure measurements to characterize the structure of these solutions at the nanoscale and larger dimensions. Both the polymer and ion concentrations were varied over a broad concentration range. The experimental results were complemented by molecular dynamics simulations of a coarse-grained bead-spring model that includes an explicit solvent.

We present SANS results for bottlebrush solutions. The influences of the polymer concentration and ion concentration are studied. A comparison is made between the effects of mono- and divalent salts (sodium chloride and calcium chloride) on the SANS profiles. DLS is used to quantify the effects of the polymer concentration and ionic environment on the dynamic response of bottlebrush polymer solutions. Then, the results of osmotic pressure measurements are presented to quantify binary and ternary interpolymer interaction strengths, where the osmotic data are analyzed in terms of the Flory-Huggins theory. The osmotic compressibility of the bottlebrush solution determined from macroscopic osmotic pressure measurements is compared with that estimated from SANS. We also compare our experimental findings with the results of molecular dynamics simulations to interpret the main trends in our measurements.

## MATERIALS AND METHODS

### Synthesis of bottlebrush polymers

Poly(*tert*-butyl acrylates) (PtBAs) with three different chain lengths were synthesized via atom transfer radical polymerization (ATRP) according to a previously reported procedure.<sup>12</sup> In a typical experiment, a 25 ml Schlenk tube was charged with methyl  $\alpha$ -bromoisobutyrate (0.071 ml, 0.540 mmol), *t*BA (4.0 ml, 27.0 mmol), DMF (1.0 ml), CuBr<sub>2</sub> (1.8 mg, 0.008 mmol), and PMDETA (0.035 ml, 0.160 mmol). The solution was degassed by three freeze-pump-thaw cycles. During the final cycle, the Schlenk tube was filled with nitrogen, and CuBr (23.0 mg, 0.160 mmol) was

quickly added to the frozen reaction mixture. The Schlenk tube was sealed, evacuated, and backfilled with nitrogen three times. The tube was thawed to room temperature, and the polymerization was conducted at 65 °C. After 45 min, the polymerization was stopped at 50% conversion. The mixture was filtered through neutral alumina and precipitated into cold 20% H<sub>2</sub>O/MeOH; this procedure was repeated twice.

PtBAs were then end-functionalized with norbornene according to a previously reported procedure.<sup>12</sup> A 25 ml Schlenk tube was charged with PtBA-Br (260 mg, 0.0867 mmol), toluene (0.6 ml), DMSO (0.6 ml), *exo*-norbornenyl-functionalized nitroxide radical (37.5 mg, 0.0867 mmol), and Me<sub>6</sub>TREN (0.026 ml, 0.095 mmol). The solution was degassed by three freeze-pump-thaw cycles. During the final cycle, the Schlenk tube was filled with nitrogen, and CuBr (14.0 mg, 0.095 mmol) was added to the frozen reaction mixture. The Schlenk tube was sealed, evacuated, and backfilled with nitrogen three times. The tube was thawed to room temperature; the mixture was stirred at room temperature for 2 h, then filtered through neutral alumina, and precipitated into cold 20% H<sub>2</sub>O/MeOH once.

The bottlebrush PtBAs with three different backbone chain lengths were synthesized via living ring-opening metathesis polymerization (ROMP) of PtBA. In a typical experiment, a 20 ml vial was charged with 500 mg of macromonomer and purged with N<sub>2</sub>. The desired amount of degassed, anhydrous THF ([MM] = 0.05M) was added to dissolve the macromonomer. The desired amount of catalyst was injected into the macromonomer solution to initiate the polymerization. The solution was stirred at room temperature under nitrogen. After the polymerization was complete, the reaction mixture was quenched with one drop of ethyl vinyl ether.

Bottlebrush PtBAs were then hydrolyzed and neutralized to produce negatively charged polyelectrolytes. 2 g of PtBA was dissolved in dichloromethane (15 ml). Trifluoroacetic acid (15 ml) was then added to the solution, and the mixture was stirred at room temperature for 2 days. The polymers were precipitated in ether and redissolved in saturated NaHCO<sub>3</sub>. The resulting solutions were then dialyzed against deionized water for 3 days and lyophilized to obtain the desired polyelectrolytes as white powders.

### Preparation of polymer solutions

We prepared polymer solutions by dissolving the sodium salt of the polymers in water (for osmotic and light scattering measurements) or in D<sub>2</sub>O (for SANS measurements). The polymer concentration ranged between 1% and 20% m/m. (Polymer concentrations are given in terms of polymer mass relative to the mass of the entire solution expressed as a percentage.) Concentrations of added sodium chloride were varied between 0 mM and 400 mM, and the concentration of calcium chloride was varied between 0 mM and 100 mM. In all samples, the pH was adjusted to 7. The samples were heated (70 °C for 5 h–6 h) to ensure faster homogenization. All measurements were made at 25.0 ± 0.1 °C.

### Small-angle neutron-scattering measurements

SANS measurements were made on the NGB 10m Small Angle Neutron Scattering instrument at NIST, Gaithersburg MD, using a

wavelength of  $\lambda = 8 \text{ \AA}$ , with wavelength spread  $\Delta\lambda/\lambda = 0.13$ . Two sample-detector distances were used, 4 m and 10 m, corresponding to an explored wave vector range  $0.003 \text{ \AA}^{-1} < q < 0.2 \text{ \AA}^{-1}$ , where  $q = (4\pi/\lambda) \sin(\theta/2)$ , with  $\theta$  being the scattering angle. The sample temperature during the experiment was maintained at  $25 \pm 0.1 \text{ }^\circ\text{C}$ . After radial averaging, corrections for incoherent background, detector response, and cell window scattering were applied. The neutron-scattering intensities were calibrated using water.<sup>13</sup>

### Dynamic light scattering

DLS measurements were made using a precision detector—Expert Laser Light Scattering DLS Workstation (Bellingham, MA)—equipped with a HeNe laser working at 698 nm. Measurements were performed in the angular range of  $45^\circ$ – $120^\circ$  with accumulation times of 200 s. Absolute intensities were obtained by normalizing with respect to toluene.

### Osmotic pressure measurements

The osmotic pressures of the polymer solutions were determined by bringing them to equilibrium with polyvinyl alcohol (PVA) hydrogel filaments of known osmotic swelling pressure.<sup>14,15</sup> The size of the PVA gels was measured by optical microscopy after equilibration in the bottlebrush solution ( $\approx 1$  day). The polymer solution was separated from the gel by a semi-permeable membrane that prevented the penetration of the polymer molecules into the swollen PVA gel. The osmotic pressure measurements were made at  $25 \pm 0.1 \text{ }^\circ\text{C}$ .

### Simulation methods

We employed a bead–spring model of Lennard-Jones (LJ) segments bound by stiff harmonic bonds suspended in explicit LJ solvent particles, some of which are charged to represent counter-ions. The particular model has been utilized in previous studies to probe the association of polyelectrolyte chains in solution, and here, we briefly outline the model and the relevant methods.<sup>16–18</sup> All macro-ion segments, dissolved ions, and solvent particles are assigned the same mass  $m$ , size  $\sigma$ , strength of interaction  $\epsilon$ , and all dissolved ions are monovalent. We set  $\epsilon$  and  $\sigma$  as the units of energy and length; the cutoff distance for the LJ interaction potential is  $r_c = 2.5 \sigma$ . The parameters between different particle types are set equal to unity, except for the energy interaction parameter between the solvent particles and the counter-ions  $\epsilon_{c,s}$ , which reflects the solvent affinity of the counter-ions. In previous papers, we considered the experimental estimate of  $\epsilon_{c,s}/\epsilon = 1.25$  for  $\text{Na}^+$ .<sup>19,20</sup> All polyelectrolyte bottlebrush polymers have a linear chain with a backbone of length of  $N_b = 40$  segments. There are  $f$  side chains of length  $M = 12$  segments, bonded and distributed uniformly along the backbone. Thus, the total number of segments per bottlebrush polymer is  $M_w = fM + N_b = 520$  segments. We also consider the linear polyelectrolyte chains of  $M_w = 41$  segments. Each segment of the linear chain polyelectrolytes and each segment of the side chain in the case of bottlebrush polyelectrolytes carry a  $-e$  charge per segment, where  $e$  is the elementary charge and the total polyelectrolyte charge is  $Z_p = -fM e$  for bottlebrushes and  $Z_p = -M_w e$  for linear chains. The bonds between

polymer segments are connected via a stiff harmonic spring,  $V_H(r) = k(r - l_0)^2$ , where  $l_0 = \sigma$  is the equilibrium length of the spring and  $k = 1000 \epsilon/\sigma^2$  is the bond spring constant.

The system is composed of a total of  $N = 252\,000$  particles in a periodic cube of side  $L$  and volume  $V$ . The system includes  $N_p$  polyelectrolyte chains and  $N_+ = N_p|Z_p/e|$  counter-ions; the number of neutral particles is  $N_0 = N - N_+ - N_p M_w$ , and we define the charge fraction as  $\varphi = (N_+ + N_p|Z_p/e|)/N$ . Each system has an overall neutral total charge. All charged particles interact via the Coulomb potential with a cutoff distance  $r_{c,c} = 10 \sigma$ , and the particle–particle particle-mesh method is used for distances  $r > r_{c,c}$ . The Bjerrum length was set equal to  $l_B = e^2/(\epsilon_s kT) = 2.4 \sigma$ , where  $T$  is the temperature,  $k$  is Boltzmann's constant, and  $\epsilon_s$  is the dielectric constant of the medium. Our simulations were equilibrated under constant pressure and constant temperature conditions, i.e., reduced temperature  $k_B T/\epsilon = 0.75$  and reduced pressure  $\langle P \rangle \approx 0.02$ , and production runs were performed at constant temperature and constant volume, maintained at equilibrium by a Nosé–Hoover thermostat. Typical simulations equilibrate for  $40\,000 \tau$ , and data are accumulated over a  $20\,000 \tau$  interval, where  $\tau = \sigma(m/\epsilon)^{1/2}$  is the time unit; the time step used was  $\Delta t/\tau = 0.005$ .

## RESULTS AND DISCUSSION

### Bottlebrush preparation and chemical characterization

We used ROMP of macromonomers (MMs) to synthesize the desired brush polymers with well-controlled lengths of the backbone and side chains and guaranteed complete grafting of one side chain per backbone repeat unit. The dispersity of the brush polymers resulting from this synthetic strategy often relies on the quality of MMs used.<sup>21</sup> To synthesize PtBA MMs, we used a nitroxide radical coupling (NRC) strategy that we recently reported to couple a nitroxide-appending norbornene (NBE) to the chain end of PtBA prepared using ATRP.<sup>12</sup> We synthesized PtBA with degrees of polymerization (DP) of 12, 25, and 40 via ATRP. NRC gave quantitative chain end functionalization with NBE as revealed by <sup>1</sup>H-NMR spectroscopy. We then subjected these NBE-functionalized MMs to various amounts of third generation Grubbs catalyst (G3) to initiate ROMP at  $[\text{NBE}] = 0.05\text{M}$  in THF at room temperature, targeting the backbone DP of 50, 80, and 400. The resulting brush polymers all showed low dispersity and MWs that are close to the expected values (Table 1). The resulting polymers were then deprotected using trifluoroacetic acid and neutralized with  $\text{NaHCO}_3$  to produce negatively charged poly(sodium acrylate) brush polymers (Scheme 1). To investigate the differences between architectures (linear and bottlebrush), we also synthesized a linear polymer with pendent carboxylate groups using ROMP to represent the same backbone structure but with only one carboxylate group per backbone repeat unit (Scheme 1). Thus, a series of well-defined polyelectrolytes were obtained with various main chain and side chain lengths, but identical polymer main chain and side chain structures (Table 1).

We aim to access the solution properties of our model synthetic polyelectrolyte brush polymers with a combination of SANS, DLS, osmotic pressure measurements, and molecular dynamics simulations. As a benchmark, we compared results in each case to the

TABLE I. Characterization of polymers.

Samples	Side chain			Bottlebrush		
	$M_n$ (kDa) <sup>a</sup>	$S^b$	$D_M^a$	$M_n$ (kDa) <sup>a</sup>	$M^c$	$D_M^a$
M400/S40	3.8	40	1.08	1975	400	1.25
M80/S40	3.8	40	1.08	347	80	1.10
M50/S40	3.8	40	1.08	204	50	1.03
M400/S25	2.7	25	1.04	1510	400	1.08
M400/S12	1.5	12	1.10	678	400	1.13
M400/S0				Linear polymer		
				104	400	1.08

<sup>a</sup>Determined by GPC in THF on two PolyPore columns using RI and MALLS detectors.

$D_M$  is the polydispersity of the polymer.

<sup>b</sup>DP of side chains.

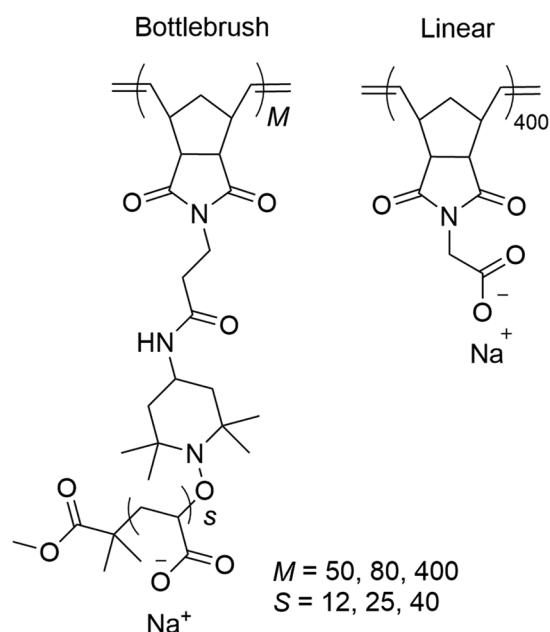
<sup>c</sup>DP of polymer main chains.

solution properties of a linear chain polyelectrolyte with the same backbone structure and sodium carboxylate charges.

### Static scattering observations

SANS measurements yield essential information on the organization of the polymer molecules over a broad range of length scales extending from that of the segment length, which is on the order of 1 nm to ~50 nm. We next compare the SANS results obtained for linear and bottlebrush polyelectrolytes.

Figure 1 shows our SANS data of the solutions M400/S0 and M400/S40 without added salt at four different polymer



**SCHEME 1.** Chemical structures of bottlebrush and linear poly(sodium acrylates) studied in this work.  $M$  is the DP of the polymer main chain, and  $S$  is the DP of side chains.

concentrations. The SANS profiles of all solutions exhibit similar characteristic features. At low  $q$  ( $< 0.02 \text{ \AA}^{-1}$ ), there is a distinct upturn of the scattering intensity. Similar behavior has been observed in the SANS profiles of many other solutions of charged polymers, both flexible polyelectrolytes (e.g., polystyrene sulfonate) and relatively rigid molecules such as charged polysaccharides and DNA. This scattering feature is usually attributed to large-scale clusters (multichain domains), the size of which exceeds the resolution of the SANS experiment.<sup>22–24</sup> In the low  $q$ -region, the slope is close to  $-4$  (Porod's law scaling), indicating that the clusters have sharp boundaries.<sup>23</sup> In the intermediate  $q$ -region ( $0.02 \text{ \AA}^{-1} < q < 0.2 \text{ \AA}^{-1}$ ), a correlation peak is observed due to long-range Coulombic interactions among the charged polymer chains. The peak position  $q^*$  is defined by the arrangement of the polymer molecules in the solution. It defines the average distance between the scattering centers,  $d = 2\pi/q^*$ . In the present solutions,  $q^*$  is displaced toward higher values of  $q$  with increasing polymer concentration. Scaling theory predicts that the position of the “polyelectrolyte peak” varies as  $q^* \sim c^m$ , where  $m = 1/3$  in dilute solutions and  $m = 1/2$  in semidilute solutions.<sup>25,26</sup> The insets in Figs. 1(a) and 1(b) show that  $q^*$  exhibits a power law behavior with an exponent  $m \approx 0.45$ , in reasonable agreement with the scaling model. The corresponding distances span from 6.53 nm ( $c = 4\% \text{ m/m}$ ) to 3.54 nm ( $c = 16\% \text{ m/m}$ ) for the linear polymer and from 18.47 nm ( $c = 4\% \text{ m/m}$ ) to 9.96 nm ( $c = 16\% \text{ m/m}$ ) for the bottlebrush polymer. We note that at high  $q$  ( $> 0.1 \text{ \AA}^{-1}$ ), all curves exhibit a linear behavior with a slope close to  $-1$ , reflecting the rod-like local structure of the chains.

Figure 1 also shows that the qualitative nature of  $I(q)$  is unaffected by the change of the polymer architecture, although the “polyelectrolyte peak” of the bottlebrush polymer is appreciably sharper than its linear polymer counterpart, indicating that the nearest neighbor distance is more uniform than in the corresponding solution of the linear polymer. Furthermore, the height of the linear chain polyelectrolyte peak increases strongly with the polymer concentration. In contrast, in solutions of the bottlebrush polymer, the peak height weakly decreases with increasing polymer concentration. The insets in these figures show that the peak position in both polymer systems changes with a concentration scaling exponent less than  $1/2$  in magnitude. Scaling arguments for polyelectrolyte solutions predict a concentration exponent of  $1/2$ , but these arguments assume that polyelectrolyte solutions are structurally homogeneous. By contrast, many small angle neutron and x-ray scattering measurements made on polyelectrolyte solutions indicate the presence of large excess scattering at low  $q$ , corresponding to large scale heterogeneities. Moreover, the measured exponents, while often near  $1/2$ , are observed to lie in a range between  $1/3$  and  $1/2$  in synthetic linear polymers, biopolymers, dendrimers, and proteins.<sup>27–33</sup> The polyelectrolyte peak is also found for synthetic clay particles in solution, which can be thought of as two-dimensional polyelectrolyte polymers.<sup>34</sup> Recently, Chremos and Douglas<sup>17</sup> demonstrated from molecular dynamics simulations with the explicit solvent that the degree of ion solvation can significantly influence the scaling exponent, causing it to range from  $1/2$  in the case of weak counter-ion solvation to nearly 0 for strong counter-ion solvation, implying that the strength of ion solvation plays a key role in the organization of the polyelectrolytes in solution. Selective polymer solvation can also make a significant effect on

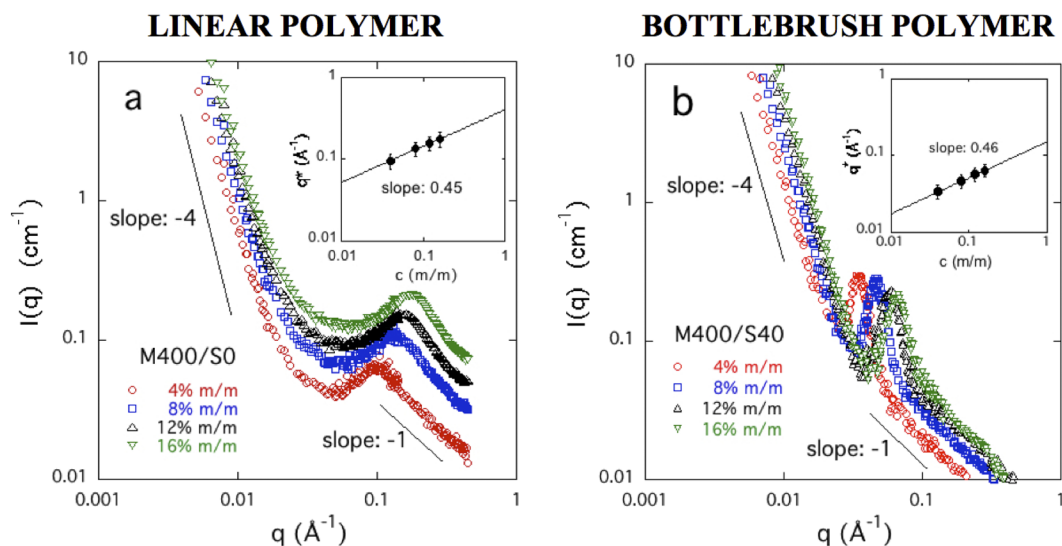


**FIG. 1.** SANS profiles of salt-free solutions of the linear M400/S0 (a) and bottlebrush M400/S40 (b) polymers at different concentrations. Insets show the variation of the polyelectrolyte peak position  $q^*$  with the polymer concentration. The data uncertainties in the insets are estimated by one standard deviation of the linear regression fit parameters.

polyelectrolyte solution structural organization (see the section titled Results and Discussion).

We next consider the comparative solution morphology of linear and bottlebrush polyelectrolytes obtained from molecular dynamics simulations, where the modeling includes an explicit solvent and ion solvation, as described in the section titled Simulation methods. In general, the SANS intensity of solutions of monodisperse particles is given as  $I(q) = c M \Delta\rho^2 P(q) S(q)$ , where  $c$  is the concentration,  $M$  is the molecular mass,  $\Delta\rho^2$  is the contrast factor,  $P(q)$  is the particle form factor, and  $S(q)$  is the particle structure factor.  $P(q)$  is defined by the size and shape of the particles, while  $S(q)$  contains information on their relative positions.

Here, we calculate the structural correlations between the polyelectrolytes as follows:

$$S_c(q) = \frac{1}{N} \left\langle \sum_{j=1}^N \sum_{k=1}^N \exp[-i \mathbf{q} \cdot (\mathbf{r}_j - \mathbf{r}_k)] \right\rangle, \quad (1)$$

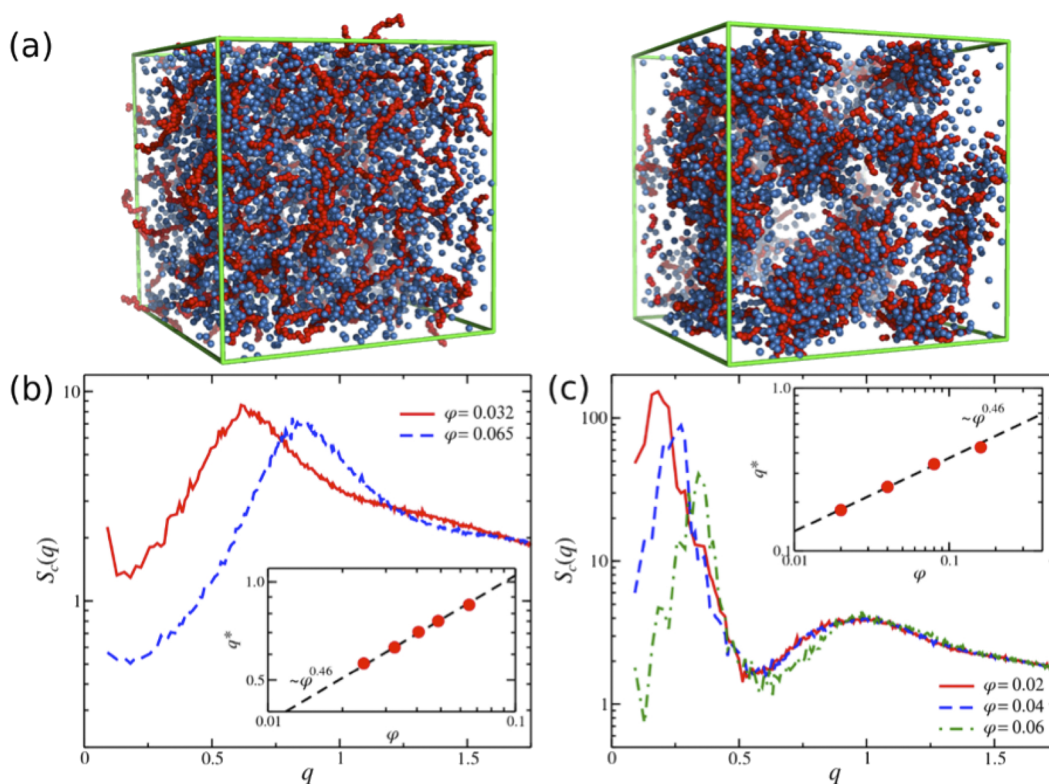
where  $i = \sqrt{-1}$ ,  $\mathbf{r}_j$  is the position of the polymer segment,  $\langle \dots \rangle$  denote the time average, and  $N$  is the total number of polyelectrolyte segments.  $S_c(q)$  contains information for both intermolecular distances between the chains and intramolecular distances between the polyelectrolyte segments. The bottlebrush polyelectrolyte solutions exhibit two peaks. The polyelectrolyte peak occurs at smaller  $q$ -values compared to linear chain systems, suggesting that the inter-polymer distance is influenced by the length of side chains, which will be discussed below. For both the linear chain and bottlebrush polyelectrolyte solutions shown in Fig. 2, the polyelectrolyte peak shifts to a larger  $q$ -value with increasing polymer concentration, corresponding to a smaller interchain domain spacing. The scaling of  $q^*$  with polymer concentration found in our simulation

model is in good agreement with experiments (see the insets in Figs. 1 and 2, where the concentration scaling of polyelectrolyte  $q^*$  is illustrated).

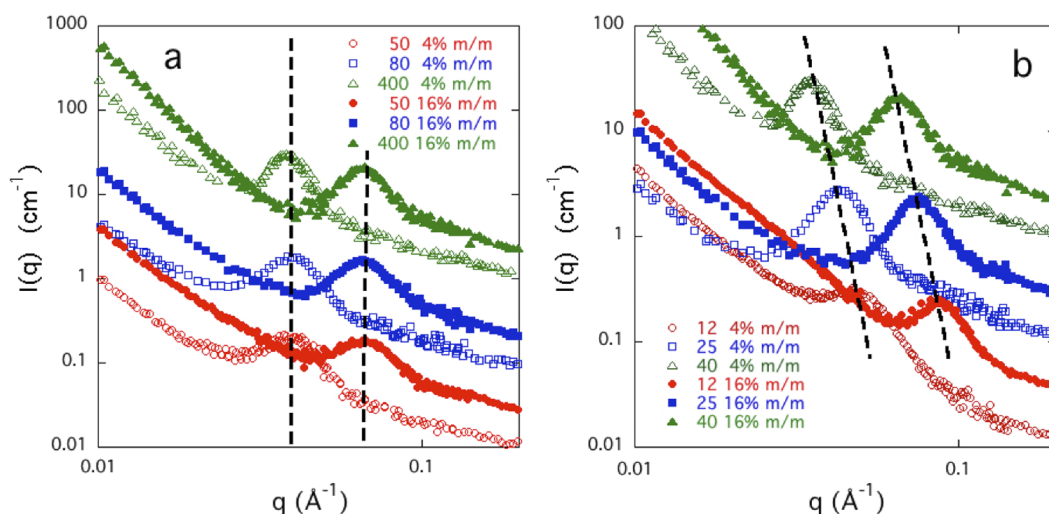
The influence of the bottlebrush topology on the SANS data is shown in Fig. 3. In Fig. 3(a), we show the bottlebrush solution data for various backbone lengths, i.e., for different numbers of repeating units: 50, 80, and 400, at constant side chain length (40 repeating units). For clarity, the scattering intensity was multiplied by a factor of 10, as the chain length is increased. The results shown for the lowest (4% m/m) and highest (16% m/m) polymer concentrations indicate that in salt free solutions, the scattering curves are qualitatively similar to those of the linear polymers. The scattering peak appears at the same value of  $q$ , i.e., at the constant side chain length, the average distance between the scattering centers is practically unaffected by the length of the main polymer chain.

Figure 3(b) shows the SANS profiles of bottlebrush polymers having constant backbone length (400 repeating units) with different side chain lengths ( $S = 12, 25,$  and  $40$  repeating units). In this case, the peak position progressively shifts toward lower  $q$  values as the side chain length increases implying that the average distance between the scattering centers increases.

Figure 4 shows the variation of the distance between the scattering centers as a function of the side chain length.  $d$  displays a power law scaling with the number of repeating units in the side chains,  $S$ . The resulting scaling  $d \sim S^\alpha$  is practically independent of the polymer concentration, and the value of the exponent  $\alpha \approx 0.2$  is similar to values observed in dendrimer solutions.<sup>35</sup> A similar scaling relation has been observed in neutral bottlebrush polymer melts, where the inter-backbone distance scales with the side chain length with an exponent less than the random coil value of  $1/2$ .<sup>36</sup>



**FIG. 2.** (a) Computer simulation screenshots of salt-free polyelectrolyte solutions for linear chains (left) and bottlebrush (right) polymers. The polyelectrolyte segments are indicated as red spheres and the counter-ions by blue spheres, and the solvent molecules are not shown to aid the visualization of the polymers and counter-ions. Solution structure factor  $S_c(q)$  of (b) linear chains and (c) bottlebrush polyelectrolyte solutions at different polymer concentrations. The insets show the polyelectrolyte peak position as a function of the polymer volume fraction  $\phi$ . The scaling of the polyelectrolyte peak accords with the experimental observations described in Fig. 1.



**FIG. 3.** SANS profiles of 4% m/m and 16% m/m solutions of bottlebrush polymers with different backbone lengths (a) at constant side chain length ( $S = 40$ ) and with different side chain lengths (b) at constant backbone length ( $M = 400$ ), where  $S = 12, 25,$  and  $40$ . For clarity, the scattering intensities are multiplied by a factor of 10, as the chain length increases. The dashed lines show the variation of the peak position for the different solutions.

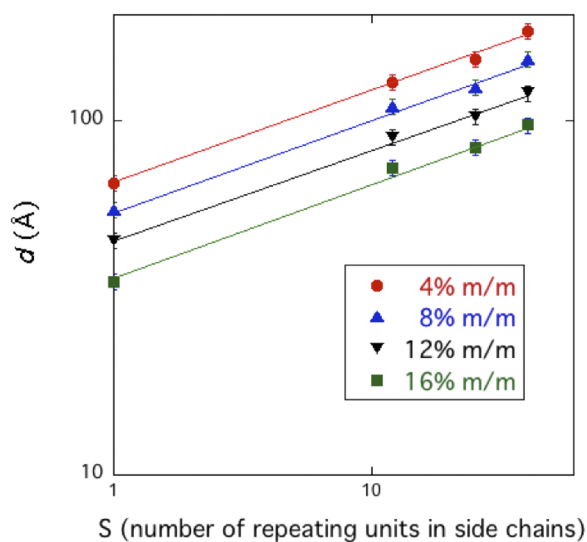


**FIG. 4.** Dependence of the average distance between the scattering centers  $d$  on the number of repeating units in the side chains at different polymer concentrations. Number of repeating units in the backbone of the bottlebrush: 400. Linear chains are formally treated as bottlebrushes with  $S = 1$ . Continuous lines are guides for the eye. The data uncertainties are estimated by one standard deviation of the linear regression fit parameters.

Figure 5 illustrates the effect of added salt on the SANS profiles of bottlebrush polymers. The main scattering features remain qualitatively similar to those of the salt free solutions: (i) all solutions show a  $q^{-4}$  scaling at low  $q$ , corresponding to dense structures with sharp interfaces, and (ii) at high  $q$ , the SANS curves exhibit a  $q^{-1}$  dependence, corresponding to the locally rod-like structure of the individual polyelectrolyte chains. Increasing the ionic strength,

however, progressively screens the electrostatic repulsion between the charged groups on the polymer backbone, as indicated by the gradual decrease in the peak height. Interestingly, the scattering profile of the sample containing 200 mM NaCl is practically indistinguishable from that containing 50 mM  $\text{CaCl}_2$ .

### Dynamic light scattering

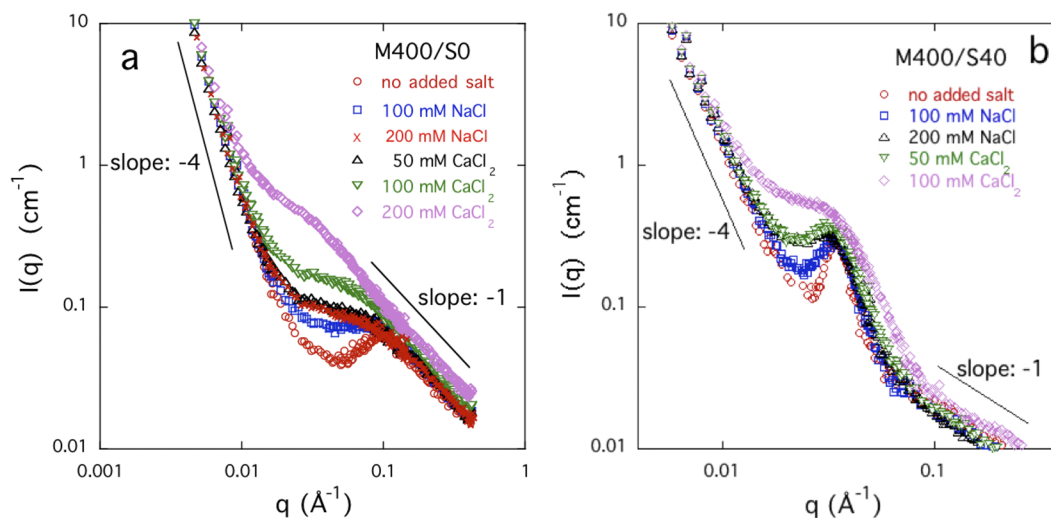
So far, we have discussed the static properties of linear and bottlebrush polymer solutions both in salt-free solution and in the presence of added salt. In what follows, we make an attempt to identify the consequences of the bottlebrush architecture on the dynamic properties measured by dynamic light scattering. We present side by side the results obtained for the linear polymer (M400/S0) and for the bottlebrush polymer with the longest side chain (M400/S40).

Figure 6 shows the typical field correlation functions measured in 4% m/m solutions at five different scattering angles  $\theta$ . Each curve displays a double relaxation process in which the two relaxation rates are separated by approximately two orders of magnitude. The field correlation function  $g(t)$  can be described by the sum of two terms,

$$g(t) = a \exp(-\Gamma_{\text{fast}} t) + (1 - a) \exp[-(\Gamma_{\text{slow}} t)^\mu]. \quad (2)$$

In Eq. (2), the fit parameters  $a$  and  $(1 - a)$  correspond to the relative intensities of the fast and slow relaxation modes, respectively,  $\Gamma_{\text{fast}}$  and  $\Gamma_{\text{slow}}$  being the corresponding relaxation rates, and the exponent  $\mu$  ( $\approx 2/3$ ) is a constant. Inset (a) in Fig. 6 shows that the fast relaxation rate  $\Gamma_{\text{fast}}$  is proportional to  $q^2$ , i.e., the fast mode is a diffusive process.

The inset (b) of Fig. 6 indicates that  $\Gamma_{\text{slow}}$  also varies as  $q^2$ . There has been much speculation in the literature about the origin of the slow mode [second term in Eq. (2)].<sup>37,38</sup> It is likely that the slow relaxation component is due to the internal modes of large



**FIG. 5.** SANS profiles of 4% m/m solutions of linear (a) and bottlebrush (b) polymer in the presence of added salts.

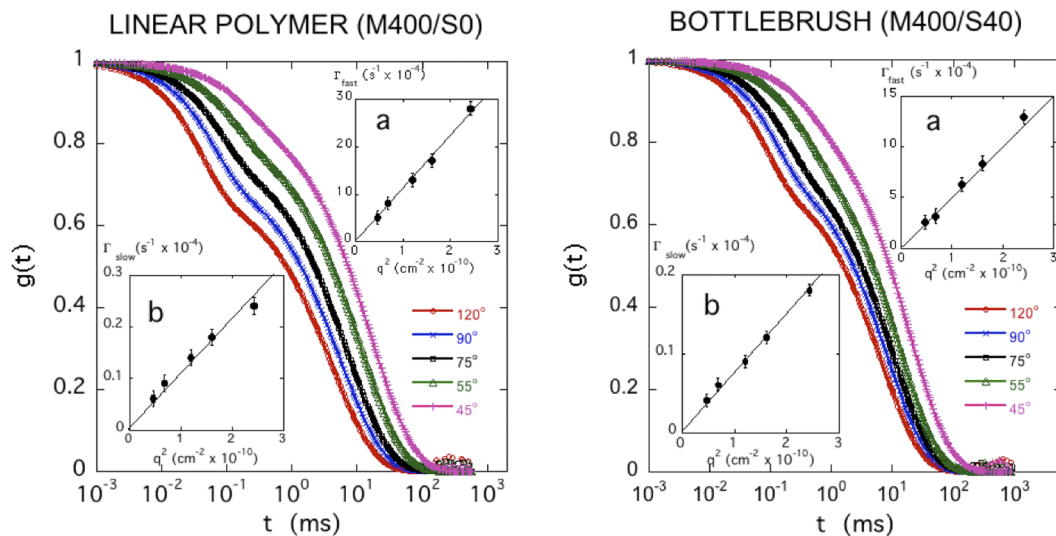


**FIG. 6.** Angular dependence of the field correlation function  $g(t)$  of light scattered by solutions of linear (left) and bottlebrush (right) polymers at  $c = 4\%$  m/m. Inset (a): variation of the fast relaxation rate  $\Gamma_{\text{fast}}$  with  $q^2$ . Inset (b): variation of the slow relaxation rate  $\Gamma_{\text{slow}}$  with  $q^2$ . The data uncertainties in the insets are estimated by one standard deviation of the linear regression of fit parameters.

clusters. For such modes, for which no unique correlation length can be identified, the relaxation process can be represented by a stretched exponential decay with an exponent  $\mu \approx 2/3$ . The trend in Fig. 6 shows that the intensity of the slow component ( $1 - a$ ) increases with decreasing scattering angle  $\theta$ , indicating that the clusters are large. This finding is consistent with the increase in intensity of the SANS signal at small values of  $q$ . The physical meaning of the slow mode is not generally agreed upon. Previous studies have shown that  $\Gamma_{\text{slow}}$  is related to the presence of aggregates or large domains in polyelectrolyte solutions, the size and shape of which may vary over time. Because of the uncertainties in the interpretation of  $\Gamma_{\text{slow}}$ , we exclude the slow relaxation mode from the further analysis.

The behaviors of the linear and bottlebrush polymers are qualitatively similar; however, the numerical values of both  $\Gamma_{\text{fast}}$  and  $\Gamma_{\text{slow}}$  are greater for the linear polymer by approximately a factor of two. This finding implies that the bottlebrush topology (the presence of side chains) slows down the collective dynamics of the polyelectrolyte solution.

In Fig. 7, we show  $g(t)$  at a scattering angle  $\theta = 90^\circ$  for solutions of linear and bottlebrush molecules at different polymer concentrations. The curves exhibit the same double relaxation behavior, as shown in Fig. 6, and are analyzed in terms of Eq. (2). The analysis reveals that with increasing polymer concentration  $\Gamma_{\text{fast}}$  becomes faster [inset (a)] and  $\Gamma_{\text{slow}}$  becomes slower [inset (b)], and the relative intensity ( $1 - a$ ) of the latter component increases. A similar decrease in  $\Gamma_{\text{slow}}$  with increasing polymer concentration has been reported for semi-dilute solutions of other linear polyelectrolytes.<sup>28,38</sup>

Ion-induced structural changes also affect the dynamic properties of polyelectrolyte solutions. Figure 8 illustrates the effect of the  $\text{CaCl}_2$  concentration on  $g(t)$  at 4% m/m polymer concentration. The

measurements were made at  $\theta = 90^\circ$ . With increasing  $\text{CaCl}_2$  concentration,  $\Gamma_{\text{fast}}$  becomes slower [inset (a)] and  $\Gamma_{\text{slow}}$  becomes faster [inset (b)], while the relative intensity of the slow component gradually decreases from 0.74 to 0.50 for the linear polymer and from 0.76 to 0.52 for the bottlebrush polymer.

The fast relaxation rate  $\Gamma_{\text{fast}}$  describes the relaxation of the thermodynamic concentration fluctuations, which is governed by the collective diffusion coefficient  $D_{\text{fast}}$ ,<sup>25</sup>

$$D_{\text{fast}} = \Gamma_{\text{fast}}/q^2. \quad (3)$$

The values of the diffusion coefficients obtained from  $\Gamma_{\text{fast}}$  are plotted as a function of the polymer concentration in Fig. 9. In both systems, over the entire concentration range ( $2\% \text{ m/m} \leq c \leq 16\% \text{ m/m}$ ),  $D_{\text{fast}}$  exhibits a power law dependence of the form

$$D_{\text{fast}} = D_0 c^m, \quad (4)$$

with  $m = 0.49$  (linear polymer) and  $m = 0.53$  (bottlebrush polymer). The experimental exponent is lower than that predicted by the scaling theory ( $m = 3/4$ ) for neutral polymer solutions of infinite molecular weight in good solvent conditions. Similar values for the exponent have been reported for solutions of linear polyelectrolytes.<sup>38,39</sup> The deviation of  $m$  from the neutral polymer value may be attributed to long range interactions in charged systems.

The correlation length of a polymer solution  $\xi$  describes the extent of the spatial range of thermodynamic concentration fluctuations and is defined by the Stokes–Einstein relationship<sup>25</sup>

$$\xi = \frac{kT}{6\pi\eta D_{\text{fast}}}, \quad (5)$$

where  $\eta$  is the viscosity of the solvent,  $k$  is the Boltzmann constant, and  $T$  is the absolute temperature. In inset (a) of Fig. 9, the

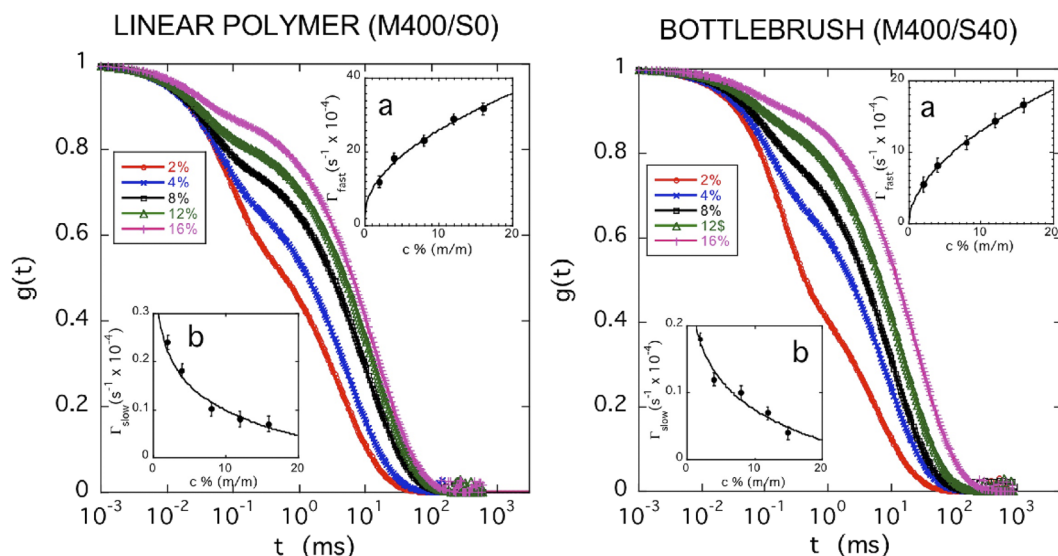


**FIG. 7.** Concentration dependence of the field correlation function  $g(t)$  of light scattered by solutions of linear (left) and bottlebrush (right) polymers at scattering angle  $\theta = 90^\circ$ . Inset (a): variation of the fast relaxation rate  $\Gamma_{fast}$  with  $c$ . Inset (b): variation of the slow relaxation rate  $\Gamma_{slow}$  with  $c$ . The data uncertainties in the insets are estimated by one standard deviation of the linear regression fit parameters.

DLS dynamic correlation length  $\xi$  is compared with the distance  $d$  observed by SANS. The latter is about two times greater than  $\xi$ , but the concentration dependences of these two lengths are similar.

Inset (b) in Fig. 9 illustrates the effect of  $\text{CaCl}_2$  on  $D_{fast}$  at 4% m/m polymer concentration. Addition of  $\text{CaCl}_2$  progressively decreases the value of  $D_{fast}$ . The continuous lines are the fits to a power law with respect to the  $\text{CaCl}_2$  concentration in which

the exponents are  $-0.45$  (linear polymer) and  $-0.41$  (bottlebrush polymer).

### Osmotic properties

In the semi-dilute concentration range, the osmotic pressure of a neutral polymer solution  $\Pi$  can be described by a modified Flory-Huggins equation,<sup>40,41</sup>

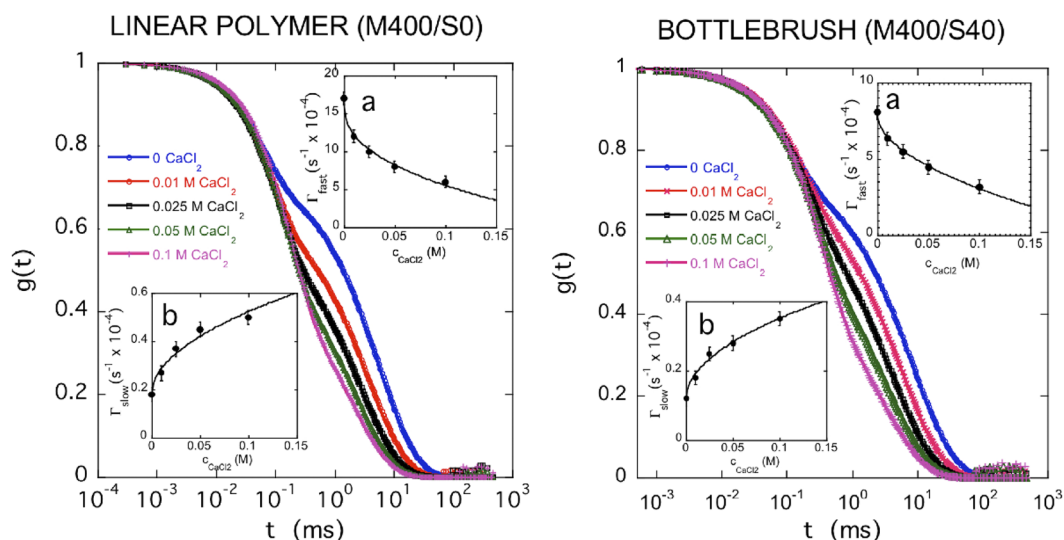


**FIG. 8.** Dependence of the field correlation function  $g(t)$  of light scattered by 4% m/m solutions of linear (left) and bottlebrush (right) polymers on the  $\text{CaCl}_2$  concentration at scattering angle  $\theta = 90^\circ$ . Inset (a): variation of the fast relaxation rate  $\Gamma_{fast}$  with  $c_{\text{CaCl}_2}$ . Inset (b): variation of the slow relaxation rate  $\Gamma_{slow}$  with  $c_{\text{CaCl}_2}$ . The data uncertainties in the insets are estimated by one standard deviation of the linear regression fit parameters.

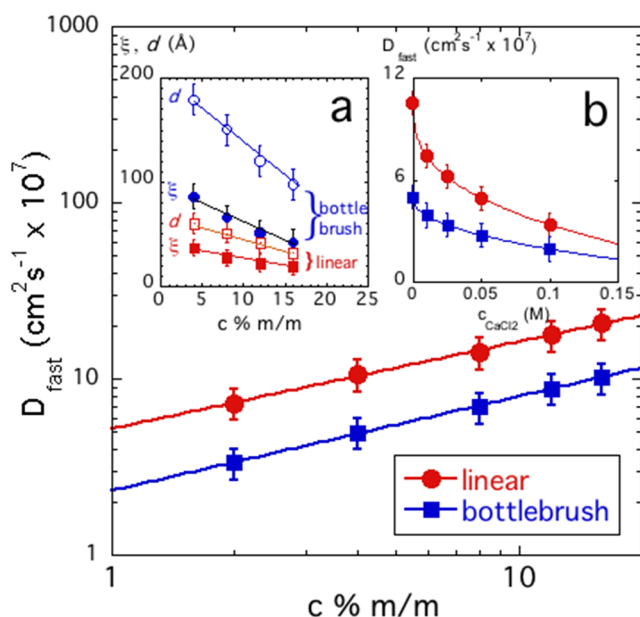


**FIG. 9.** Dependence of  $D_{\text{fast}}$  on the polymer concentration  $c$  in salt-free solutions. The slopes of the power law fits are 0.49 (linear polymer) and 0.53 (bottlebrush polymer). Inset: (a) characteristic length  $d$  from SANS (open symbols) and correlation length  $\xi$  from DLS (filled symbols) as a function of the polymer concentration for solutions of linear and bottlebrush polymers. (b) Variation of  $D_{\text{fast}}$  of 4% m/m for solutions of linear (circles) and bottlebrush (squares) polymers with  $\text{CaCl}_2$  concentration. Data uncertainties are estimated by one standard deviation of the linear regression fit parameters.

$$\Pi = - (RT/V_1) [\ln(1 - \varphi) + (1 - 1/P)\varphi + \chi_0 \varphi^2 + \chi_1 \varphi^3], \quad (6)$$

where  $\varphi$  is the volume fraction of the polymer,  $V_1$  is the molar volume of the solvent,  $P$  is the degree of polymerization,  $R$  is the gas constant,  $T$  is the absolute temperature, and  $\chi_0$  and  $\chi_1$  are interaction parameters describing binary and ternary interactions, respectively, and these are related to the second and third osmotic virial coefficients. In general, these interaction parameters can be expected to depend on added salt type and concentration, and other factors that influence molecular rigidity and effective interpolymer interaction strength.

In polyelectrolyte solutions, an additional term is also present due to electrostatic effects. However, molecular dynamics simulations demonstrated that the osmotic pressure of neutralized polyelectrolyte solutions can be satisfactorily described by Eq. (6) because under equilibrium conditions, the electrostatic contribution to the osmotic pressure is largely compensated by the counterion excluded-volume contribution.<sup>42</sup> Therefore, we adopt Eq. (6) to describe the concentration dependence of  $\Pi$  for the present solutions.

Figure 10 shows the variation of the osmotic pressure as a function of the polymer volume fraction for solutions of bottlebrush polymers with increasing backbone length [at constant side-chain length,  $S = 40$ , Fig. 10(a)] and with increasing side-chain length [at constant backbone length,  $M = 400$ , Fig. 10(b)]. We find that

$\Pi$  decreases with increasing polymer molecular weight. The continuous curves are the least squares fits of Eq. (6) to the data; the insets show  $\chi_0$  and  $\chi_1$  obtained from the fits. It can be seen that  $\chi_0$  is practically unaffected by the bottlebrush topology. However,  $\chi_1$  exhibits different behaviors in the different sets of samples; it decreases with increasing backbone length and increases with increasing side chain length. Since bottlebrushes are relatively rigid structures, it is reasonable to assume that higher order interactions decrease with increasing backbone length relative to the length of side chains. However, with increasing side chain length, the ternary effects are expected to become more pronounced, as shown in Fig. 10(b).

Figure 11 illustrates the effect of  $\text{CaCl}_2$  on the  $\Pi$  vs  $\varphi$  plots for the solutions of two polymers: one without side chains (sample: M400/S0, Fig. 11(a)) and the other with the longest side chains (M400/S40, Fig. 11(b)). In both systems, the effect of  $\text{Ca}^{2+}$  ions is qualitatively similar: it only weakly affects the interaction parameter  $\chi_0$ , while the interaction parameter  $\chi_1$  strongly increases with increasing  $\text{CaCl}_2$  concentration. This finding indicates that attractive ternary interactions are increased as  $\text{Ca}^{2+}$  ions screen the electrostatic repulsion between the polymer chains, leading to enhanced interchain association. The effect of  $\text{Ca}^{2+}$  ions is apparently more pronounced in the solution of the bottlebrush polymer, but the trend is qualitatively similar. An increase in  $\chi_1$  with increasing  $\text{CaCl}_2$  concentration has been reported for other polyelectrolyte systems.<sup>41,43</sup> Of course, other effects such as residual electrostatic interactions, structural flexibility of the polymer chains, hydrophobic interactions (i.e., the full complexity of polyelectrolyte molecules), probably also influence  $\chi_1$ . Further experimental, theoretical, and computational investigations of this interaction parameter are warranted.

### Comparison between microscopic and macroscopic thermodynamic observations

To reveal the relationship between microscopic structure and thermodynamic properties, we combined scattering measurements probing the system at high resolution with macroscopic osmotic observations.

The neutron scattering intensity  $I(q)$  of a polyelectrolyte solution can be described by<sup>44</sup>

$$I(q) = \frac{A}{[1 + (qL)^2]^{1/2} [1 + (qR)^2]}, \quad (7)$$

where  $L$  is the correlation length,  $R$  is the effective cross-sectional radius of the polymer chain, and  $A$  is a constant, the value of which is proportional to the squared contrast factor between the polymer unit and the solvent molecule. In semidilute polymer solutions,  $L$  is frequently interpreted as the “mesh size” (average distance between neighboring polymer molecules). Such interpretation applies both to the case of polymers uniformly distributed in solution or within polymer supramolecular assemblies in solution.

In polymer solutions, in which large-scale structures (e.g., clusters) are present, the description of the scattering response requires additional terms. In polyelectrolyte solutions, molecular associations give rise to an extra scattering contribution at small angles, and the scattering intensity takes the form of a power law,

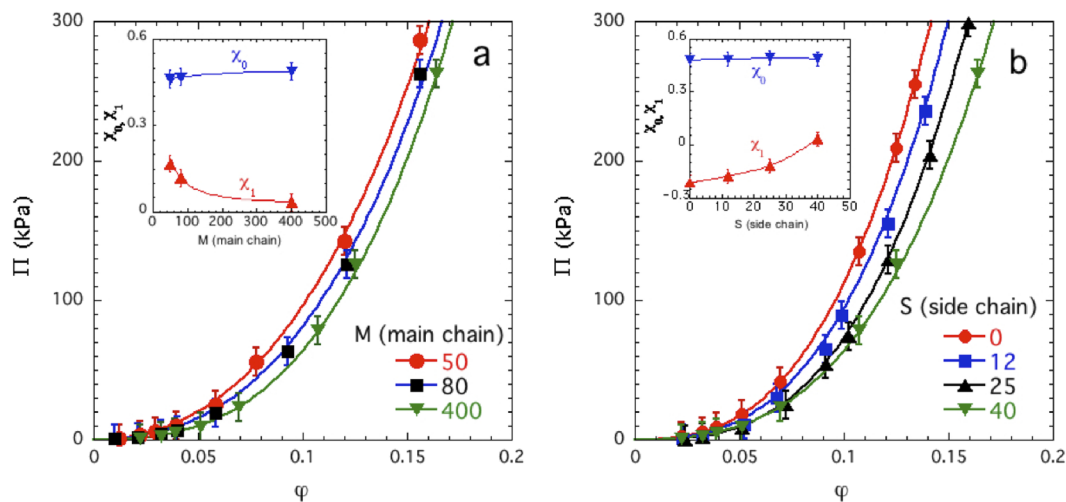


**FIG. 10.** Osmotic pressure  $\Pi$  as a function of polymer volume fraction  $\phi$  for solutions of bottlebrush polymers with different main chain lengths (a) and side chain lengths (b). The continuous lines through the data points are the least squares fits of Eq. (6) to the experimental data. The insets show the variation of  $\chi_0$  and  $\chi_1$  as a function of the number of monomer units in the main chain (a) and in the side chains (b). The data uncertainties are estimated by one standard deviation of the linear regression fit parameters.

$$I_{\text{cluster}}(q) = B q^{-m}, \quad (8)$$

where  $B$  is a constant and  $m > 3$ .<sup>44</sup> The total scattering intensity thus becomes

$$I(q) = \frac{A}{[1 + (qL)^2]^{1/2} [1 + (qR)^2]} + B q^{-m}. \quad (9)$$

The scattering intensity at  $q = 0$  is defined as

$$A = \Delta \rho^2 \frac{kT\phi}{\partial \Pi / \partial \phi}. \quad (10)$$

Based on the Flory–Huggins theory,  $\partial \Pi / \partial \phi$  is given by

$$\partial \Pi / \partial \phi = \phi \left( \frac{RT}{V_1} \right) \left( \frac{1}{1 - \phi} + \frac{1}{P} - 2\chi_0 - 3\chi_1 \phi \right). \quad (11)$$

Equations (10) and (11) allow us to compare the scattering intensities obtained from SANS in the limit  $q \rightarrow 0$  and independent

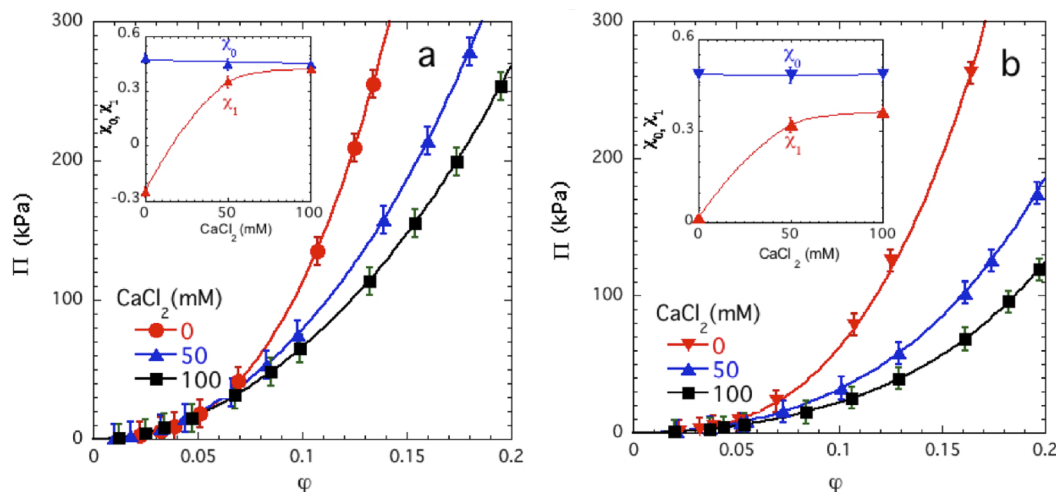


**FIG. 11.** Osmotic pressure  $\Pi$  as a function of polymer volume fraction  $\phi$  for solutions of linear [M400/S0], (a) and bottlebrush polymers [M400/S40], (b) in  $\text{CaCl}_2$  solutions of different concentrations. The continuous lines through the data points are the least squares fits of Eq. (6) to the experimental data. The insets show the variation of  $\chi_0$  and  $\chi_1$  as a function of the  $\text{CaCl}_2$  concentration of the solutions. The data uncertainties are estimated by one standard deviation of the linear regression fit parameters.

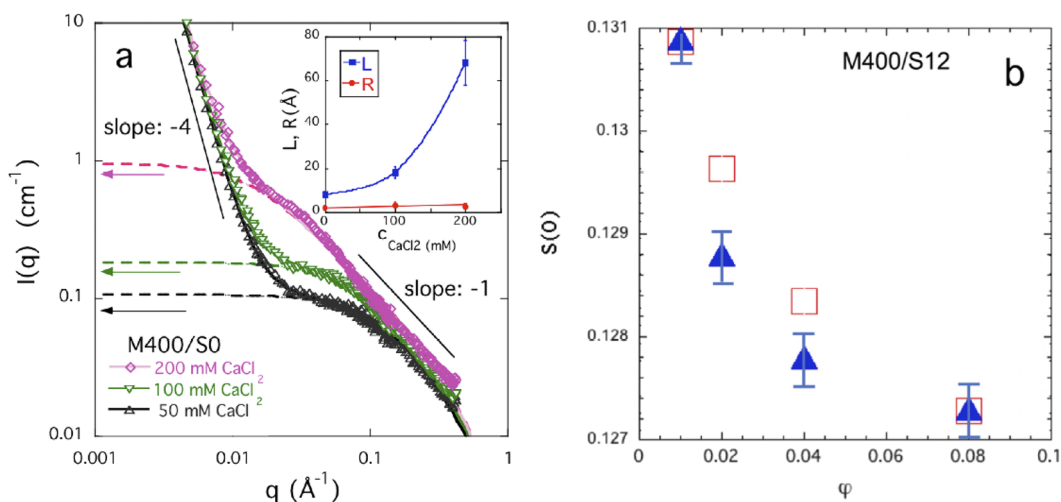


**FIG. 12.** (a) SANS profiles of 4% m/m polymer solutions containing different amounts of added salts. The continuous curves are the least squares fits of Eq. (9) to the SANS data; the dashed curve is the first term of Eq. (9). The arrows show the intensities calculated from osmotic pressure measurements. Inset:  $L$  and  $R$  as a function of the  $\text{CaCl}_2$  concentration. (b) Structure factor in the long wavelength limit,  $S(q \rightarrow 0)$ , obtained from molecular dynamic simulation at salt-free conditions (filled triangles) and osmotic pressure measurements (open squares) as a function of polymer volume fraction  $\phi$  for sample M400/S12. The data uncertainties in (b) are estimated by one standard deviation of the linear regression fit parameters.

estimates of  $S(0)$  from osmotic pressure measurements. This comparison is made in Fig. 12(a), which shows the scattering profiles of three solutions with the fitting functions [Eq. (9)] through the data points, together with the thermodynamic component (dashed lines) corresponding to the first term of Eq. (9). The horizontal arrow directed to the y axis indicates the scattering intensity calculated by Eqs. (10) and (11). The amplitude of the concentration fluctuations obtained from the decomposition of the SANS signal appears to be slightly larger than that estimated from osmotic pressure measurements. Similar agreement between results from these two independent techniques has been reported for different polymer gels.<sup>44–47</sup>

The structure factor at  $q = 0$  is given as<sup>48,49</sup>,

$$S(q \rightarrow 0) = T\phi \frac{\partial \phi}{\partial \Pi}. \quad (12)$$

The concentration dependence of  $S(0)$  can be obtained independently from molecular dynamics simulations using of the following relationship that holds at equilibrium:

$$S(0) = \rho kT \kappa_T, \quad (13)$$

where  $\rho$  is the solution density and  $\kappa_T$  is the isothermal compressibility defined as  $\kappa_T = -\frac{1}{V} \left( \frac{\partial V}{\partial P} \right)_T$ . We performed simulations at different pressures ( $\langle P \rangle \approx 0, 0.1, 0.2,$  and  $0.3$ ), and  $V$  decreased linearly with increasing pressure. Once we obtained the values of  $\kappa_T$  by fitting to  $V$  at different pressures, then  $S(0)$  is obtained with the use of Eq. (13). We repeated the process for different polymer concentrations, as illustrated in Fig. 12(b). Our findings accord well with data estimated from osmotic pressure measurements.

## CONCLUSIONS

Static and dynamic scattering and osmotic pressure measurements reveal remarkably similarities between the solution behavior of linear and bottlebrush polymers, but there are also some notable differences. In particular, SANS measurements show that the solutions of both linear and bottlebrush polymers exhibit the usual polyelectrolyte correlation peak at a position on the order of nanometers, which is practically independent of the length of the bottlebrush chain backbone. With increasing length of the side chains of the bottlebrush polymers, the peak position is shifted toward lower values of  $q$ , indicating that the average distance between the scattering centers increases. As the concentration of the added salt increases, the peak gradually disappears, and at high ion concentrations, only a shoulder can be observed. The effect of divalent counter-ions on the shape of the scattering curves is more prominent than that of the monovalent ions, but the overall trends are similar.

Dynamic light scattering measurements reveal that the relaxation rate of the bottlebrush polymer solution is slower by approximately a factor of 2 than that of the corresponding linear polymer. In both systems, two distinct relaxation modes are clearly distinguishable. The fast relaxation rate  $\Gamma_{\text{fast}}$  is diffusive and is governed by the thermal concentration fluctuations. The slow mode  $\Gamma_{\text{slow}}$  reflects the presence of large clusters that give rise to strong excess scattering at low  $q$  in the SANS measurements. The relaxation rate of the fast mode increases with increasing polymer concentration and decreases with increasing  $\text{CaCl}_2$  concentration, while  $\Gamma_{\text{slow}}$  becomes slower with increasing polymer concentration and faster with increasing  $\text{Ca}^{2+}$  ion concentration. Over the whole range of polymer and ion concentrations explored in the present study,  $D_{\text{fast}}$  displays power law dependences on both variables.

The power law exponent of the dependence of  $D_{\text{fast}}$  on the polymer concentration is smaller than the exponent predicted by the scaling theory for neutral polymer solutions.

It is found that the concentration dependence of the osmotic pressure of bottlebrush solutions can be satisfactorily described by a modified Flory–Huggins equation containing two interaction parameters. The interpolymer interaction parameter  $\chi_0$  is only slightly affected by the topology of the molecules, while  $\chi_1$  decreases with the length of the main chain and increases with the length of the side chains. Addition of  $\text{CaCl}_2$  only weakly affects the binary interaction parameter  $\chi_0$ , and  $\chi_1$  exhibits a strong increase with increasing  $\text{CaCl}_2$  content, reflecting the growth of attractive ternary intermolecular interactions with increasing divalent salt concentration.

A comparison was made between the experimental results obtained by SANS and osmotic pressure measurements as well as molecular dynamic simulations. Overall, the agreement between the experimental findings and simulation data is remarkably good considering the coarse-grained nature of the simulation model.

## ACKNOWLEDGMENTS

This research was supported by the Intramural Research Program of the NICHD, NIH. We acknowledge the support of the National Institute of Standards and Technology, U.S. Department of Commerce, in providing the neutron research facilities used in this work. Use of the NGB 10m SANS instrument was supported by the NIST nSoft Consortium.

## DATA AVAILABILITY

The data that support the findings of this study are available from the corresponding authors upon reasonable request.

## REFERENCES

- <sup>1</sup>S. J. Dalsin, M. A. Hillmyer, and F. S. Bates, “Molecular weight dependence of zero-shear viscosity in atactic polypropylene bottlebrush polymers,” *ACS Macro Lett.* **3**, 423–427 (2014).
- <sup>2</sup>X. Li, S. L. Prukop, S. L. Biswal, and R. Verduzco, “Surface properties of bottlebrush polymer thin films,” *Macromolecules* **45**, 7118–7127 (2012).
- <sup>3</sup>G. Sun, S. Cho, C. Clark, S. V. Verkhoturov, M. J. Eller, A. Li, A. Pavia-Jiménez, E. A. Schweikert, J. W. Thackeray, P. Trefonas, and K. L. Wooley, “Control of polymer architectures by living ring-opening metathesis copolymerization,” *J. Am. Chem. Soc.* **135**, 4203–4206 (2013).
- <sup>4</sup>J. A. Johnson, Y. Y. Lu, A. O. Burts, Y.-H. Lim, M. G. Finn, J. T. Koberstein, N. J. Turro, D. A. Tirrell, and R. H. Grubbs, “Core-clickable PEG-branch-azide bivalent-bottle-brush polymers by ROMP: Grafting-through and clicking-to,” *J. Am. Chem. Soc.* **133**, 559–566 (2010).
- <sup>5</sup>S. L. Pesek, X. Li, B. Hammouda, K. Hong, and R. Verduzco, “Small-angle neutron scattering analysis of bottlebrush polymers prepared via grafting-through polymerization,” *Macromolecules* **46**, 6998–7005 (2013).
- <sup>6</sup>K. L. Beers, S. G. Gaynor, K. Matyjaszewski, S. S. Sheiko, and M. Möller, “The synthesis of densely grafted copolymers by atom transfer radical polymerization,” *Macromolecules* **31**, 9413–9415 (1998).
- <sup>7</sup>L. Ng, A. J. Grodzinsky, P. Patwari, J. Sandy, A. Plaas, and C. Ortiz, “Individual cartilage aggrecan macromolecules and their constituent glycosaminoglycans visualized via atomic force microscopy,” *J. Struct. Biol.* **143**, 242–257 (2003).
- <sup>8</sup>F. Horkay, P. J. Basser, A.-M. Hecht, and E. Geissler, “Gel-like behavior in aggrecan assemblies,” *J. Chem. Phys.* **128**, 135103–135107 (2008).
- <sup>9</sup>H. Watanabe, Y. Yamada, and K. Kimata, “Roles of aggrecan, a large chondroitin sulfate proteoglycan, in cartilage structure and function,” *J. Biochem.* **124**, 687–693 (1998).
- <sup>10</sup>P. J. Basser, R. Schneiderman, R. A. Bank, E. Wachtel, and A. Maroudas, “Mechanical properties of the collagen network in human articular cartilage as measured by osmotic stress technique,” *Arch. Biochem. Biophys.* **351**, 207–219 (1998).
- <sup>11</sup>S. Das, M. Banik, G. Chen, S. Sinha, and R. Mukherjee, “Polyelectrolyte brushes: Theory, modelling, synthesis and applications,” *Soft Matter* **11**, 8550–8583 (2015).
- <sup>12</sup>Y. C. Teo and Y. Xia, “Facile synthesis of macromonomers via ATRP–nitroxide radical coupling and well-controlled brush block copolymers,” *Macromolecules* **52**, 81–87 (2019).
- <sup>13</sup>P. Lindner, “Water calibration at DLL verified with polymer samples,” *Appl. Cryst.* **33**, 807–811 (2000).
- <sup>14</sup>M. Nagy and F. Horkay, “A simple and accurate method for the determination of solvent activity in swollen gels,” *Acta Chim. Acad. Sci. Hung.* **104**, 49–61 (1980).
- <sup>15</sup>H. Vink, “Precision measurements of osmotic pressure in concentrated polymer solutions,” *Eur. Polym. J.* **7**, 1411–1419 (1971).
- <sup>16</sup>A. Chremos and J. F. Douglas, “Counter-ion distribution around flexible polyelectrolytes having different molecular architecture,” *Soft Matter* **12**, 2932–2941 (2016).
- <sup>17</sup>A. Chremos and J. F. Douglas, “Polyelectrolyte association and solvation,” *J. Chem. Phys.* **149**, 163305 (2018).
- <sup>18</sup>A. Chremos and J. F. Douglas, “Counter-ion solvation and anomalous low-angle scattering in salt-free polyelectrolyte solutions,” *J. Chem. Phys.* **147**, 241103 (2017).
- <sup>19</sup>M. Andreev, J. J. de Pablo, A. Chremos, and J. F. Douglas, “Influence of ion solvation on the properties of electrolyte solutions,” *J. Phys. Chem. B* **122**, 4029–4034 (2018).
- <sup>20</sup>M. Andreev, A. Chremos, J. de Pablo, and J. F. Douglas, “Coarse-grained model of the dynamics of electrolyte solutions,” *J. Phys. Chem. B* **121**, 8195–8202 (2018).
- <sup>21</sup>Y. C. Teo and Y. Xia, “Importance of macromonomer quality in the ring-opening metathesis polymerization of macromonomers,” *Macromolecules* **48**, 5656–5662 (2015).
- <sup>22</sup>J. S. Higgins and R. S. Stein, “Recent developments in polymer applications of small-angle neutron, X-ray and light scattering,” *J. Appl. Cryst.* **11**, 346–375 (1978).
- <sup>23</sup>O. Glatter and O. Kratky, *Small Angle X-Ray Scattering* (Academic Press, London, 1982).
- <sup>24</sup>M. Muthukumar, “50th anniversary perspective: A perspective on polyelectrolyte solutions,” *Macromolecules* **50**, 9528–9560 (2017).
- <sup>25</sup>P. G. de Gennes, *Scaling Concepts in Polymer Physics* (Cornell University Press, Ithaca, NY, 1979).
- <sup>26</sup>P. G. de Gennes, P. Pincus, R. M. Velasco, and F. Brochard, “Remarks on polyelectrolyte conformation,” *J. Phys.* **37**, 1461–1473 (1976).
- <sup>27</sup>F. Horkay and B. Hammouda, “Small-angle neutron scattering from typical synthetic and biopolymer solutions,” *Colloid Polym. Sci.* **286**, 611–620 (2008).
- <sup>28</sup>Y. Zhang, J. F. Douglas, B. D. Ermi, and E. J. Amis, “Influence of counterion valency on the scattering properties of highly charged polyelectrolyte solutions,” *J. Chem. Phys.* **114**, 3299–3313 (2001).
- <sup>29</sup>R. Borsali, H. Nguyen, and R. Pecora, “Small-angle neutron scattering and dynamic light scattering from a polyelectrolyte solution: DNA,” *Macromolecules* **31**, 1548–1555 (1998).
- <sup>30</sup>W. Essafi, F. Lafuma, and C. E. Williams, “Effect of solvent quality on the behaviour of highly charged polyelectrolytes,” *J. Phys. II* **5**, 1269–1275 (1995).
- <sup>31</sup>W. F. Reed, “Observation of liquidlike correlations of polyelectrolytes under high-shear conditions,” *J. Chem. Phys.* **100**, 7825–7827 (1994).
- <sup>32</sup>A. Ramzi, R. Scherrenberg, J. Joosten, P. Lemstra, and K. Mortensen, “Structure–property relations in dendritic polyelectrolyte solutions at different ionic strength,” *Macromolecules* **35**, 827–833 (2002).

- <sup>33</sup>A. Mourchid, A. Delville, J. Lambard, E. Lecolier, and P. Levitz, "Phase diagram of colloidal dispersions of anisotropic charged particles: Equilibrium properties, structure, and rheology of laponite suspensions," *Langmuir* **11**, 1942–1950 (1995).
- <sup>34</sup>G. Nisato, R. Ivkov, and E. J. Amis, "Structure of charged dendrimer solutions as seen by small-angle neutron scattering," *Macromolecules* **32**, 5895–5900 (1999).
- <sup>35</sup>S. I. Yun, R. M. Briber, R. A. Kee, and M. Gauthier, "Small-angle neutron scattering of arborescent polystyrene-graft-poly(2-vinylpyridine) copolymers," *Polymer* **44**, 6579 (2003).
- <sup>36</sup>A. Chremos and J. F. Douglas, "Polyelectrolyte association and solvation," *J. Chem. Phys.* **149**, 044904 (2018).
- <sup>37</sup>S. Förster and M. Schmidt, "Polyelectrolytes in solution," *Adv. Polym. Sci.* **120**, 51–133 (1995).
- <sup>38</sup>F. Horkay, P. J. Basser, A.-M. Hecht, and E. Geissler, "Chondroitin sulfate in solution: Effects of mono- and divalent salts," *Macromolecules* **45**, 2882–2890 (2012).
- <sup>39</sup>F. Horkay, P. J. Basser, D. J. Londono, A.-M. Hecht, and E. Geissler, "Ions in hyaluronic acid solutions," *J. Chem. Phys.* **131**, 184902 (2009).
- <sup>40</sup>P. J. Flory, *Principles of Polymer Chemistry* (Cornell University, Ithaca, NY, 1953).
- <sup>41</sup>F. Horkay, I. Tasaki, and P. J. Basser, "Osmotic swelling of polyacrylate hydrogels in physiological salt solutions," *Biomacromolecules* **1**, 84–90 (2000).
- <sup>42</sup>D.-W. Yin, F. Horkay, J. F. Douglas, and J. J. de Pablo, "Molecular simulation of the swelling of polyelectrolyte gels by monovalent and divalent counterions," *J. Chem. Phys.* **129**, 154902 (2008).
- <sup>43</sup>F. Horkay, "Effect of the ionic environment on the supramolecular structure and thermodynamics of DNA gels," *Macromol. Symp.* **385**, 1800199 (2019).
- <sup>44</sup>F. Horkay, P. J. Basser, A.-M. Hecht, and E. Geissler, "Ionic effects in semi-dilute biopolymer solutions: A small angle scattering study," *J. Chem. Phys.* **149**, 163312 (2018).
- <sup>45</sup>F. Horkay, A. M. Hecht, S. Mallam, E. Geissler, and A. R. Rennie, "Macroscopic and microscopic thermodynamic observations in swollen poly(vinyl acetate) networks," *Macromolecules* **24**, 2896–2902 (1991).
- <sup>46</sup>F. Horkay, A.-M. Hecht, and E. Geissler, "Fine structure of polymer networks as revealed by solvent swelling," *Macromolecules* **31**, 8851–8856 (1998).
- <sup>47</sup>F. Horkay, K. Nishi, and M. Shibayama, "Decisive test of the ideal behavior of tetra-PEG gels," *J. Chem. Phys.* **146**, 164905 (2017).
- <sup>48</sup>J. G. Kirkwood and F. P. Buff, "The statistical mechanical theory of solutions. I," *J. Chem. Phys.* **19**, 774–777 (1951).
- <sup>49</sup>P. A. Egelstaff, *An Introduction to the Liquid State* (Academic Press, New York, 1967).